doi:10.1093/brain/awr042 Brain 2011: 134; 947–958 | 947

BRAIN
A JOURNAL OF NEUROLOGY

Novel histopathologic findings in molecularly-confirmed pantothenate kinase-associated neurodegeneration

Michael C. Kruer,[1,*] Mark Hiken,[2,*] Allison Gregory,[3] Alessandro Malandrini,[4] David Clark,[2] Penny Hogarth,[3,5] Marjorie Grafe,[2] Susan J. Hayflick[3,5,6] and Randall L. Woltjer[2]

1 Divisions of Developmental Paediatrics and Paediatric Neurology, Child Development and Rehabilitation Centre, Oregon Health and Science University, Portland, OR 97239, USA
2 Section of Neuropathology, Department of Pathology, Oregon Health and Science University, Portland, OR 97239, USA
3 Department of Molecular and Medical Genetics, Oregon Health and Science University, Portland, OR 97239, USA
4 Unit of Neurometabolic Diseases, Department of Neurological, Neurosurgical and Behavioural Sciences, University of Siena, Siena 53100, Italy
5 Department of Neurology, Oregon Health and Science University, Portland, OR 97239, USA
6 Department of Paediatrics, Oregon Health and Science University, Portland, OR 97239, USA

*These authors contributed equally to this work.

Correspondence to: Susan J. Hayflick, MD,
Department of Molecular and Medical Genetics,
Oregon Health and Science University,
Richard Jones Hall Room 4541,
Mailcode L103, 3181 SW Sam Jackson Park Road,
OR 97239-3098, Portland
E-mail: hayflick@ohsu.edu

Pantothenate kinase-associated neurodegeneration is a form of neurodegeneration with brain iron accumulation, characterized by a progressive movement disorder and prominent iron deposition in the globus pallidus. Formerly referred to as Hallervorden–Spatz syndrome, the disorder was renamed pantothenate kinase-associated neurodegeneration after discovery of the causative gene, *PANK2*. Although the pathological features of clinically characterized Hallervorden–Spatz syndrome have been described, the literature is confounded by the historical use of this term for nearly all conditions with prominent basal ganglia iron accumulation and by the fact that this term encompasses a genetically heterogeneous group of disorders, now referred to as 'neurodegeneration with brain iron accumulation'. As a result, interpreting reports that precede molecular characterization of specific forms of neurodegeneration with brain iron accumulation is problematic. In the present studies, we describe neuropathological findings in six cases of molecularly confirmed pantothenate kinase-associated neurodegeneration. We identify prominent ubiquinated deposits in pantothenate kinase-associated neurodegeneration. We also characterize two distinct origins of spheroid bodies and delineate histological features of iron deposition. In so doing, we characterize fundamental features of the disease and redefine its nosological relationship to other neurodegenerative disorders.

Keywords: pantothenate kinase-associated neurodegeneration (PKAN); Hallervorden–Spatz; neuropathology; tau; α-synuclein

Abbreviations: NBIA = neurodegeneration with brain iron accumulation; PKAN = pantothenate kinase-associated neurodegeneration

Received September 23, 2010. Revised January 13, 2011. Accepted January 24, 2011

Introduction

Pantothenate kinase-associated neurodegeneration (PKAN) is a subtype of neurodegeneration with brain iron accumulation (NBIA). PKAN leads to disabling generalized dystonia and parkinsonism in affected individuals, along with a pigmentary retinopathy and a classic MRI signature: the 'eye of the tiger'. The 'eye of the tiger' is characterized by a T_2 hyperintense core surrounded by T_2 hypointensity indicating pallidal iron deposition. Associated clinical features may include dysarthria, dysphagia, Adie's pupil (Egan *et al.*, 2005) and supranuclear gaze palsy. Onset is typically in early childhood with a relentlessly progressive course. In later onset 'atypical PKAN', prominent tics and neuropsychiatric features (impulsivity, aggression, anxiety, depression, mania) often occur. Intellect is relatively spared (Freeman *et al.,* 2007).

PKAN was originally described in 1922 by Julius Hallervorden and Hugo Spatz, German Neuropathologists who were later discredited for their involvement in Nazi war crimes (Shevell and Peiffer, 2001). Available evidence indicates that Hallervorden and Spatz implicitly endorsed the mass euthanasia programmes of physical and mental 'defectives' in long-term care facilities under the Third Reich and accepted brains for study from these sources. Hallervorden–Spatz syndrome was subsequently renamed to reflect the role of the causative gene, pantothenate kinase 2 (*PANK2*) (Hayflick, 2003) after its discovery.

Additional cases were subsequently reported with more detailed descriptions of the neuropathological features of Hallervorden–Spatz syndrome (Dooling *et al.,* 1974), later referred to as NBIA (Galvin *et al*., 2000; Saitoh *et al*., 2000; Wakabayashi *et al*., 2000). Reported findings included neuroaxonal spheroids, neurofibrillary tangles and Lewy bodies, suggesting links to both Alzheimer's and Parkinson's diseases. These cases were ascertained based upon varying clinical and pathological features, most commonly the constellation of an extrapyramidal syndrome along with basal ganglia brain iron deposition and the identification of neuroaxonal spheroids. However, it is now recognized that there are at least nine distinct subtypes of NBIA (Kruer *et al*., 2010). There are also cases that lack mutations in any of the known genes, i.e. more genes await identification (Gregory *et al*., 2009). Without molecular confirmation, it is difficult to know what subtype of NBIA is described in these reports, and for this reason, the existing literature describing neuropathological features of Hallervorden–Spatz syndrome/NBIA is difficult to interpret. Histological descriptions of a heterogeneous collection of subtypes of NBIA—most called Hallervorden–Spatz syndrome—have made their way into the literature. Despite attempts to clarify the nosology of NBIA (Halliday, 1995; Zarranz *et al.*, 2006), drawing conclusions from these findings is difficult given the inconsistent features that have been reported. Furthermore, many published studies purportedly describing NBIA probably do not represent cases of PKAN (Gregory *et al*., 2009). This highlights an important gap in the field given the fundamental role that neuropathological studies play in characterizing and grouping neurodegenerative disorders (Hardy *et al*., 2009).

The first series describing the histological features of molecularly confirmed cases of a distinctive type of NBIA, phospholipase-associated neurodegeneration, was recently published (Paisan-Ruiz, *et al.,* 2010). Since detailed neuropathological studies of molecularly confirmed PKAN have not been published, we sought to characterize histological and immunohistochemical features in six such cases and to correlate our findings with neuroimaging and clinical features. Our findings differ from those previously reported in genetically uncharacterized NBIA, particularly with regard to the brain regions affected and the presence of neurofibrillary tangle and Lewy body pathology. These new findings have major implications for recrafting paradigms of the disease.

Materials and methods

Subjects were enrolled pre-mortem or after consent was obtained from surviving family members through an Oregon Health and Science University Institutional Review Board approved written consent process.

Patient histories were ascertained by a combination of direct interview, review of medical records and through correspondence with family members. Case 146 was examined by P.H. and S.J.H. After death, post-mortem brain tissue was procured at autopsy by the Oregon Brain Bank, by the University of Siena or by the National Institute of Child Health and Human Development Brain and Tissue Bank for Developmental Disorders, administered by the University of Maryland, and collected by the standardized protocol described below.

Neuroimaging

MRI scans were performed using standard clinical protocols on 1.0 or 1.5 T magnets. Images were concurrently reviewed by authors with expertise in the neuroimaging features of NBIA (P.H., M.C.K. and S.J.H.). The presence of the 'eye of the tiger' sign was determined by review of T_2- and T_2*-weighted sequences.

Molecular genetics

Primers were designed to amplify all seven exons of *PANK2* along with ~50 bp of the flanking intronic sequence, as previously described (Zhou *et al*., 2001). The resulting amplicons were sequenced in the forward and reverse directions using an ABI3700 DNA Analyzer. Complementary DNA is numbered based on the reference sequence GenBank accession number _BK000010 with the C of the CTG initiation codon designated +1.

Multiplex ligation-dependent probe amplification was performed as previously described (Haverfield *et al*., 2009), adapted for the detection of intragenic deletions and duplications in *PANK2*. Abnormal results were verified by quantitative polymerase chain reaction.

Post-mortem procedure

The brain, spinal cord, optic and/or sural nerve were fixed in 10% neutral buffered formalin for 14 days. The cerebral and cerebellar hemispheres were sectioned in the coronal plane. The brainstem and spinal cord were sectioned in the axial plane. Regions of interest were dissected into tissue blocks, processed using standard tissue processing methods, embedded in paraffin or plastic, deparaffinized and cut as 7 μM paraffin or 1 μM plastic sections.

Histology

Sections from all tissue blocks were stained with haematoxylin and eosin, and selected blocks were stained with Perls Prussian blue iron stain, Luxol fast blue, periodic acid Schiff's reaction, Congo red and Gallyas and Bielschowsky silver impregnation methods, using standard methodologies. Plastic sections were stained with toluidine blue.

Immunohistochemistry

Selected immunohistochemistry was performed after deparaffinized sections were subjected to antigen retrieval (5 min treatment at room temperature with 95% formic acid followed by incubation at 85–90°C in citrate buffer, pH 6.0 for 30 min) and stained with antibodies to tau (mouse monoclonal antibody tau-2, Sigma and anti-tau raised in chicken from Aves Labs) (both at 1:5000); ubiquitin (rabbit polyclonal antibody from Dako) (1:5000); amyloid precursor protein (rabbit polyclonal antibody from Dako) (1:3000); α-synuclein (rabbit polyclonal antibody from Thermo Scientific/Neomarkers) (1:3000); TDP-43 (rabbit polyclonal antibody from Protein Tech Group) (1:5000); Lamin A/C (Santa Cruz Biotechnology Corporation) (1:500); ferritin (rabbit anti-HFE (1:10 000 dilution, EX1 no. 137, a gift from C. Enns; original source, J. Feder) (1:1000) and FUS (rabbit polyclonal antibody from Bethyl Laboratories) (1:5000). Results were visualized with appropriate secondary antibodies and diaminobenzidine as the chromagen. Additional immunohistochemical staining was performed on Ventana Benchmark XT stainers, with cell conditioning and Ultraview (biotin-free polymer detection, Ventana) and the following antibodies: pan high- and low-molecular weight (200 and 68 kDa) neurofilament (mouse monoclonal antibody 2F11, Cell Marque) (prediluted); low-molecular weight neurofilament (mouse monoclonal antibody DA-2, Zymed) (1:1250); chromogranin A (mouse monoclonal antibody LK2H10, Ventana) (prediluted); synaptophysin (rabbit polyclonal antibody from Cell Marque) (prediluted); glial fibrillary acidic protein (mouse monoclonal antibody, clone 6F2, (Dako) (1:1200); vimentin (mouse monoclonal antibody V9, Ventana) (prediluted) and CD-163 (mouse monoclonal antibody 10D6, Vector) (1:1000).

Clinical case histories

Case 20

This patient was the younger of two sisters with PKAN previously described by Malandrini and colleagues (1995), born at term to a non-consanguineous Italian couple. The patient was globally delayed in her attainment of both cognitive/linguistic and motor milestones. By the age of 6 years, she had developed axial rigidity and oro-buccolingual and extremity dystonia. Choreoathetosis of the limbs was evident, and she had a decline in expressive speech along with neurogenic dysphagia. Funduscopic examination revealed pigmentary retinopathy. Acanthocytes were observed on peripheral blood smear. After a severe, progressive neurodegenerative course, the patient died at the age of 12 years.

Case 23

This patient was born at 35 weeks estimated gestation via C-section secondary to breech presentation after *in utero* exposure to cocaine. He was adopted shortly after birth. At 6 months, he was noted to be globally delayed in his attainment of milestones. He was subsequently diagnosed with cerebral palsy. At his best, he could walk a maximum of 15 steps and speak in three-word sentences. He suffered a stroke-like decline in function at the age of 6 years. Family history was significant for a maternal uncle with retinal disease of uncertain aetiology. His examination at the age of 10 years demonstrated pigmentary retinopathy with full extraocular movements and hypomimia. He was anarthric, but able to follow simple instructions. Severe dysphagia rendered him gastrostomy tube dependent. His tone was markedly rigid. Dystonia was severe, and manifested as retrocollis, truncal dystonia (causing him to assume a frequent 'C-shape'), a 6 Hz dystonic tremor of the chin and lower lip and left greater than right dystonia of the extremities. Toes were plantar extensor, with ankle clonus. His gait demonstrated an equinovarus posture and pes cavus. He was treated with vigabatrin as part of a study protocol to evaluate potential efficacy in dystonia, and was later treated off-label with hyperbaric oxygen. He underwent left-sided pallidotomy at the age of 10 years for treatment-refractory dystonia. A right-sided pallidotomy was performed at the age of 11 years. He died of respiratory compromise at age 20.

Case 120

The patient was born full term after an unremarkable pregnancy and delivery. She was felt to be weak in her first year of life, with a developmental plateau at about 6 months. Cerebral palsy was diagnosed at age 15 months. Pigmentary retinopathy was noted on ophthalmological examination at 2 years. Her examination at age 4 demonstrated marked generalized dystonia and dysarthria. A blood smear demonstrated acanthocytes. Family history was significant for a maternal grandmother with parkinsonism and a paternal second cousin with amyotrophic lateral sclerosis. She died at the age of 10 years.

Case 146

This patient was born at term after an uneventful pregnancy. She began to demonstrate gait problems at the age of 17 years and dystonia gradually progressed to involve her trunk and all four extremities. Pigmentary retinopathy was not observed. Her writing became progressively micrographic and illegible. She began having freezing of her gait. Dysarthria was subtle at first but became pronounced. She was felt to demonstrate some improvement in her speech quality with supplemental pantothenate (5 g/day). She developed frequent falls, and her gait deteriorated to the point that she became wheelchair dependent. An intrathecal baclofen pump was implanted at the age of 42 years for intractable dystonia, with symptomatic improvement. Family history was notable for a paternal uncle with an extrapyramidal movement disorder that began after a childhood infection. She died at the age of 48 years.

Case 158

This patient was born full term without complications. She was delayed in her attainment of motor and cognitive milestones, and was given a diagnosis of pervasive developmental disorder. She had frequent temper tantrums. At the age of three years, she began falling. Serial examinations demonstrated diffuse hypotonia that progressed to dystonia of the extremities, then to generalized dystonia. She received off-label treatment with secretin for autism and an empiric course of intravenous immunoglobulin when she began to demonstrate progressive neurological decline. Both of these interventions produced no benefit. She died at the age of 10 years.

Case 367

Limited clinical data were available for this patient, but she was known to have severe, treatment-refractory generalized dystonia with early onset. She died of respiratory complications from her disease at the age of 8 years.

Results

Mutation characterization

Homozygous or compound heterozygous mutations were identified in all six cases. These were classified as molecularly confirmed PKAN. Clinical case histories and the results of mutation screening are summarized in Table 1.

Magnetic resonance imaging features

All patients had evidence of the 'eye of the tiger' on cranial MRI, with a central T_2 hyperintense region within a hypointense globus pallidus. No patients had clear evidence of substantia nigra iron deposition. Relative sparing of the remainder of the brain was noted, and neither cerebral nor cerebellar atrophy was noted. White matter changes, observed in some forms of NBIA, were absent.

In Case 120 magnetic resonance spectroscopy centred on voxels placed in the globus pallidus demonstrated decreased *N*-acetylaspartate, suggestive of neuronal loss and an increased myoinositol peak suggestive of activated glia as has been previously reported (Kitis *et al.*, 2006).

Neuropathology

Index case (Case 146)

Gross examination

The brain weighed 1300 g fresh and was without obvious cerebral or cerebellar atrophy. No significant atherosclerosis was present. On sectioning, all ventricles were normal in size. The globus pallidus was markedly atrophic and featured rusty discoloration.

Light microscopy and immunohistochemistry

The preponderance of pathology was found in the globus pallidus, extending to a limited and variable extent to adjacent structures, while the cortex, brainstem and remaining deep grey nuclei were remarkably spared.

Histologically, the 'eye of the tiger' could be appreciated as an ovoid region of profound rarefaction centred in the globus pallidus interna (Fig. 1A; all figures are derived from the index case). This region was markedly depleted of viable neurons. Residual elements included glia, macrophages, vascular structures and axons. In addition, abundant eosinophilic spheroidal structures were appreciable in haematoxylin and eosin stained sections throughout the globus pallidus.

Large spheroidal structures with variable morphology were most abundant, although smaller, more intensely eosinophilic spheroidal structures were also observed (Fig. 1B). These 'spheroids' were found to represent two distinct populations, namely larger, granular degenerating neurons and smaller, more intensely eosinophilic dystrophic axons (further characterized below).

Most residual viable cells in the globus pallidus were glial in nature, with reactive astrocytes particularly conspicuous (Fig. 1C). Perivascular haemosiderin deposits were present and although macrophages were not conspicuous on haematoxylin and eosin sections, CD163 immunohistochemistry revealed occasional macrophages in a perivascular distribution and focal collections in the globus pallidus and internal capsule (Fig. 1D). Synaptophysin immunoreactivity was markedly depleted in the globus pallidus (Fig. 1E–G), especially centrally within the 'eye of the tiger'. These findings suggest that synaptic losses contribute especially strongly to the parenchymal loss that was apparent in many histochemical stains as generalized pallor.

Detailed examination of the brainstem, including substantia nigra, locus ceruleus and red nucleus identified only minimal loss of neuromelanin in the substantia nigra, as is frequently found with normal ageing (Fig. 1H). Lewy bodies, neuronal loss, gliosis

Table 1 Clinical and molecular features of PKAN cases

Case	Sex	Onset	Symptoms	Interventions	Age at death	Mutation	Molecular features
20	F	6 years	Dystonia Parkinsonism Pigmentary Retinopathy		12	c.1231G > A del_exon 1 (MLPA)	Missense Intragenic deletion
23	M	6 years	Dystonia Parkinsonism Pigmentary Retinopathy Nystagmus	Bilateral pallidotomies	20	1231G > A (hom)	Missense
120	F	15 months	Dystonia Pigmentary Retinopathy		10	c.943_945delCTT c.1231G > A	In-frame deletion Missense
146	F	32 years	Dystonia Parkinsonism	Pantothenate, intrathecal baclofen	48	c.1231G > A c.370A > G	Missense Missense
158	F	3 years	Dystonia Parkinsonism		10	c.1231G > A c.519C > G	Missense Missense
367	F	Unknown	Dystonia		8	c.440_441insCT c.943_945delCTT	Premature stop codon In-frame deletion

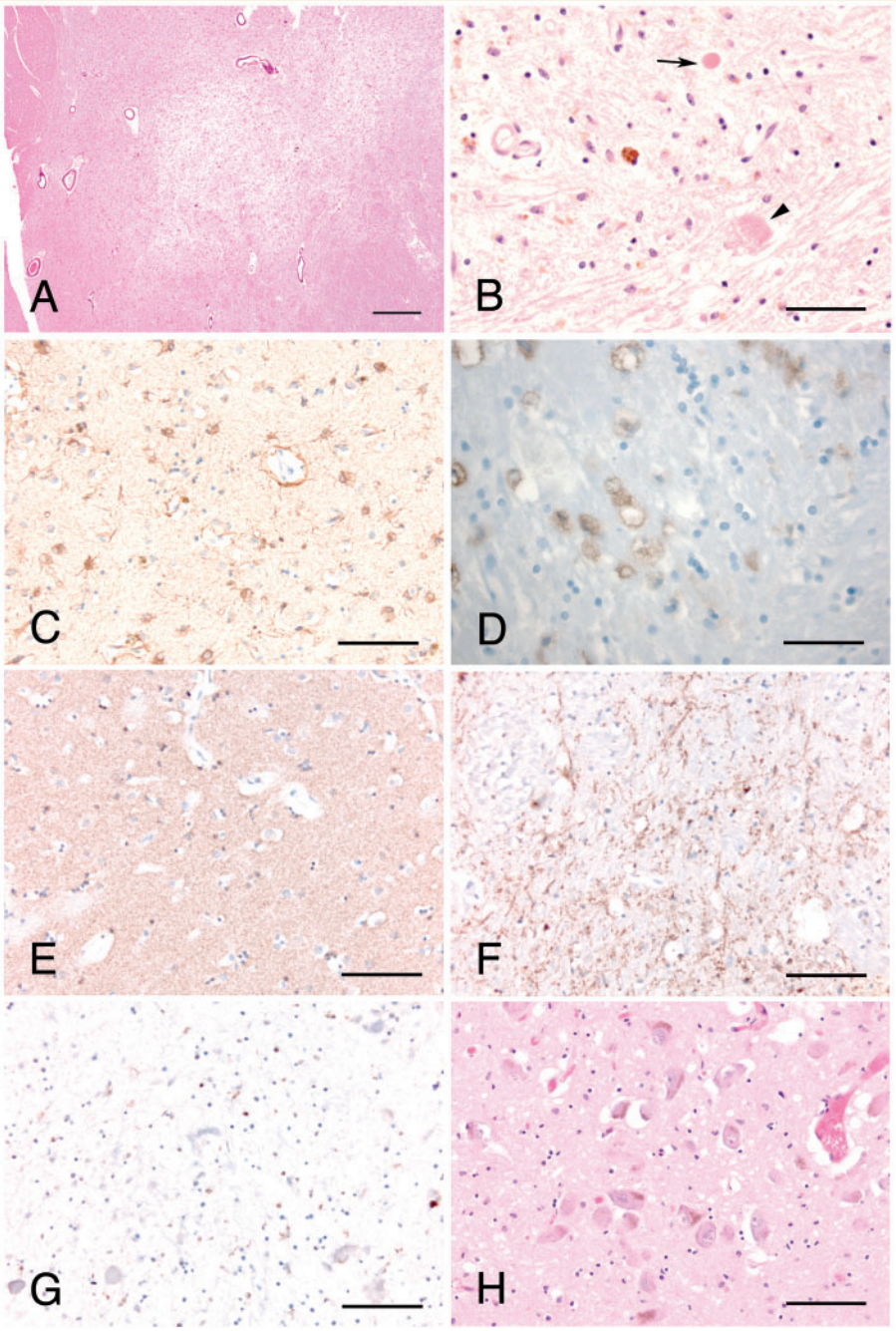

Figure 1 Histopathological features of affected tissues in PKAN. (**A**) Low-magnification view of haematoxylin and eosin stain of globus pallidus, with periodic acid Schiff's reaction stain added to highlight vascular structures, showing the rarefied area that corresponds to the 'eye of the tiger' observed radiographically (scale: 600 μm). (**B**) Both large degenerating neurons (arrowhead) and smaller neuroaxonal spheroids (arrow) were present in the globus pallidus in PKAN. Note also haemosiderin in the background (scale: 50 μm). (**C**) Glial fibrillary acidic protein immunohistochemistry of the globus pallidus, demonstrating widespread gliosis. Larger residual cells are astrocytes (scale: 100 μm). (**D**) Focal macrophage infiltrates in the globus pallidus as assessed by CD163 immunohistochemistry (scale: 50 μm). (**E**) Normal preservation of synaptic content in putamen as assessed by synaptophysin immunohistochemistry; for comparison, **E–G** were acquired at the same magnification and exposure under same light intensity (scale: 100 μm). (**F**) Relative synapse preservation more peripherally in the globus pallidus externa adjacent to the internal capsule as assessed by synaptophysin immunohistochemistry (scale: 100 μm). (**G**) Marked synapse loss in central region of globus pallidus as assessed by synaptophysin immunohistochemistry (scale: 100 μm). (**H**) Haematoxylin and eosin stain of the substantia nigra, showing good preservation of midbrain pigmented neurons (scale: 200 μm).

and iron deposition were absent. Sural and optic nerves did not demonstrate axonal spheroids or other pathological findings. Other brain regions, including cerebral cortex, hippocampus, thalamus and cerebellum also did not contain relevant pathological findings. Iron deposition was not seen outside of the globus pallidus. No amyloid was identified by Congo red stain in any section.

Iron deposition

Iron was readily appreciated in the globus pallidus on haematoxylin and eosin stains, predominantly as coarse granular haemosiderin deposits, in a perivascular distribution. More extensively distributed iron was accentuated by Perls' stain (Fig. 2A). Perls' stain highlights ferric iron (Fe^{3+}), the paramagnetic form putatively associated with hypointensity on MRI, but also demonstrates

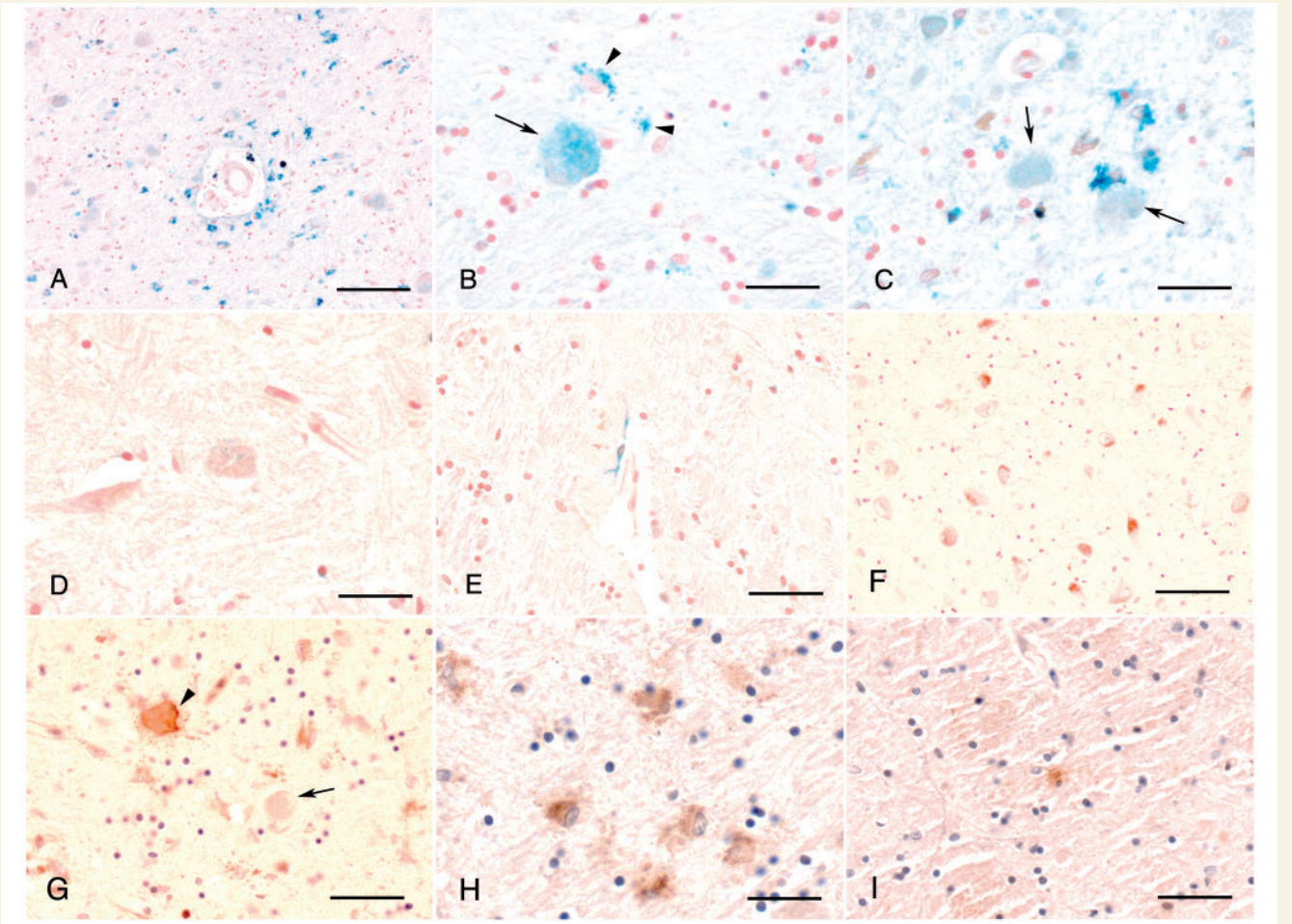

Figure 2 Iron deposits in PKAN. (**A**) Low-magnification view of the globus pallidus in PKAN, stained with Perls' stain for iron. Some perivascular accentuation of iron deposits is present, with focal collections of haemosiderin-laden macrophages as may be encountered with normal ageing (scale: 200 μm). (**B**) Perls' stain for iron, demonstrating cellular localization of iron in the globus pallidus in PKAN. Degenerating neurons with relative preservation of cytoplasm demonstrate increased cytoplasmic iron staining (arrow) compared with neurons in control globus pallidus (**D**), as well as astrocytes with more intense, dense granular accumulation of cytoplasmic iron (arrowheads). In contrast, oligodendroglia and microglia displayed no increase in iron (scale: 50 μm). (**C**) Perls' iron stain of the globus pallidus in PKAN, showing progressive decrease in iron content as neurons degenerate. Iron-positive astrocytes are more conspicuous and greatly outnumber those present in normal globus pallidus (refer to **E** for comparison). Note also increased iron diffusely present in the neuropil, manifest as a pale blue background tinge (scale: 50 μm). (**D**) Perls' stain of control globus pallidus for comparison, showing very rare neurons with detectable iron accumulation (scale: 100 μm). (**E**) Perls' stain of control globus pallidus. Rare astrocytes, predominantly in a juxtavascular distribution, were found to contain increased iron. The numbers of these were markedly less than encountered in PKAN (scale: 100 μm). (**F**) Perls' stain of the midbrain in PKAN; no detectable iron was present in the substantia nigra (scale: 200 μm). (**G**) Ferritin immunohistochemistry of the globus pallidus in PKAN, showing ferritin association of iron in some neurons, sometimes in a peripheral distribution (arrowhead). As with iron stains, ferritin staining tended not to be present in extensively degenerated neurons (arrow) (scale: 50 μm). (**H**) Ferritin immunohistochemistry of astrocytes in the globus pallidus in PKAN. As with iron stains, astrocytes demonstrated the most intense cytoplasmic ferritin (scale: 50 μm). (**I**) Ferritin immunohistochemistry of astrocytes in control globus pallidus. Very rare astrocytes display detectable labelling (scale: 100 μm).

ferrous iron to a lesser degree (Meguro *et al*., 2007). Haemosiderin deposits heterogeneously stained with Perls' stain.

Iron was present in increased amounts in some recognizable neurons in the globus pallidus, in a cytoplasmic distribution (Fig. 2B). Similar staining was absent from control brain tissue (see below). Degenerating neurons appeared as granular structures with ill-defined boundaries, as discussed below, and many of these stained less intensely for iron (Fig. 2C). Aside from perivascular iron deposits, the most intense staining in brain parenchyma was located within the cytoplasm of astrocytes (Fig. 2B and C). Age-matched controls (Fig. 2D) as well as subjects with hypertensive vasculopathy or Alzheimer's disease were also found to contain rare astrocytes in the globus pallidus with iron in this distribution, and some of these stained as intensely as some iron-positive astrocytes in PKAN (Fig. 2E). However, in PKAN, the numbers of iron-laden astrocytes were increased by at least an order of magnitude throughout the globus pallidus compared with non-PKAN brains, and the intensity of astrocyte iron staining was consistently higher in PKAN compared with controls. Significant iron staining was not present in microglia or oligodendroglial cells in PKAN. Diffusely increased iron staining of the neuropil ('iron dust') was also observed in the PKAN cases (Fig. 2C) and absent in control cases. Diffuse iron staining or increased iron in cellular elements was not identified in the midbrain (Fig. 2F).

Immunohistochemical staining for ferritin demonstrated focal staining of degenerating neurons. Some of the most strongly staining neurons showed a rim-like pattern of staining, suggesting association with plasma membranes (Fig. 2G). In general, iron staining of degenerating neurons tended to be more conspicuous than ferritin staining, suggesting the presence of at least some non-ferritin-associated iron in these structures as well. In contrast, ferritin staining of astrocytes tended to be strong and distributed in a granular pattern, similar to the results of iron staining, and suggesting that much glial iron is associated with ferritin. Finally, ferritin staining of the neuropil of the globus pallidus was diffusely increased compared with age-matched controls.

Degenerating neurons and neuroaxonal spheroids

Both large and small 'spheroids' have been described previously (Malandrini *et al*., 1995). Our findings clarify that, in fact, there are two distinct processes at work in PKAN that give rise to spheroidal structures that can be visualized in standard haematoxylin and eosin stained sections. The first, more abundant population of spheroidal structures are, in fact, degenerating neurons, while the second, rarer population appears to represent 'true' neuroaxonal spheroids, a form of swollen, dystrophic axons. Morphologically, neuroaxonal spheroids tend to be smaller, more compact and more intensely eosinophilic (Fig. 1B). A variety of immunohistochemical techniques further distinguished these two populations (see below).

Neuroaxonal spheroids

Rare, smaller eosinophilic round structures were present in the globus pallidus, the corpus callosum and the subcortical white matter. These structures were morphologically recognizable as neuroaxonal spheroids, as have been described in NBIA and in other disorders such as traumatic brain injury. Neuroaxonal spheroids were most readily detected by way of their immunoreactivity for amyloid precursor protein (Fig. 3A), which highlighted focal areas with large numbers of these structures, as well as smaller dystrophic neurons that were morphologically inconspicuous on routine haematoxylin and eosin staining (Fig. 3A). Degenerating neurons displayed variable and typically lower intensity immunoreactivity for amyloid precursor protein. Similar patterns of staining were observed for high molecular weight neurofilament (Fig. 3B).

Degenerating neurons

Numerous eosinophilic round, oval or irregularly contoured degenerating neurons were detected in the globus pallidus. Fewer numbers of these were identified in the medial putamen and in the internal capsule. These degenerating neurons ranged from 10 to 80 μm in diameter, and were characterized internally by finely granular pale eosinophilic and variable periodic acid Schiff's reaction staining. Although most degenerating neurons were negative for tau staining using the tau-2 antibody, occasional neurons displayed faint staining. A still lower degree of staining in degenerating neurons was observed with the use of anti-carboxy-terminal tau (raised in chicken) (Fig. 3C). This latter antibody displays high sensitivity and specificity to tau found within the neurofibrillary tangles of Alzheimer's disease (R. L. Woltjer, unpublished data). Staining with antibodies to chromogranin A, synaptophysin, α-synuclein, TDP-43, FUS, glial fibrillary acidic protein and vimentin was not observed within degenerating neurons, but the Gallyas silver stain focally highlighted a rim-like subset of granular elements in some instances. Most strikingly, degenerating neurons of all sizes were consistently positive for ubiquitin in a strong, uniform pattern (Fig. 3D). In contrast, neuroaxonal spheroids demonstrated substantially less staining with anti-ubiquitin immunohistochemistry.

The globus pallidus also contained occasional neurons that morphologically appeared intact but contained a diffuse mild increase in cytoplasmic ubiquitin (Fig. 3E), suggesting that accumulation of an abnormally ubiquitinated protein may precede other manifestations of degeneration in susceptible neurons. Survey of the globus pallidus revealed neurons in various stages of degeneration, confirming that cell death does not occur uniformly (Fig. 3F–H). Occasionally, the residuum of a nucleus could be detected in degenerate neurons with the use of lamin A/C immunohistochemical stains, confirming their origin in cell bodies and suggesting the possibility of a degenerative process that, in its early stages, may affect the cytoplasmic contents of neurons more than the nuclear structure (Fig. 3I).

Additional cases

Representative areas from additional cases were evaluated with haematoxylin and eosin/Luxol fast blue-stained sections, Bielschowsky and Gallyas silver stains, Perls' iron stain, and anti-tau, anti-ubiquitin, anti-α-synuclein, anti-TDP-43 and anti-FUS immunohistochemistry. Increased iron, in a distribution similar to that of the index case and degenerating neurons and neuroaxonal spheroids, was identified in the globus pallidus of all cases. These were morphologically and immunohistochemically similar to the index case. There was no clear correlation between the degree of iron deposition and other histological features, or with

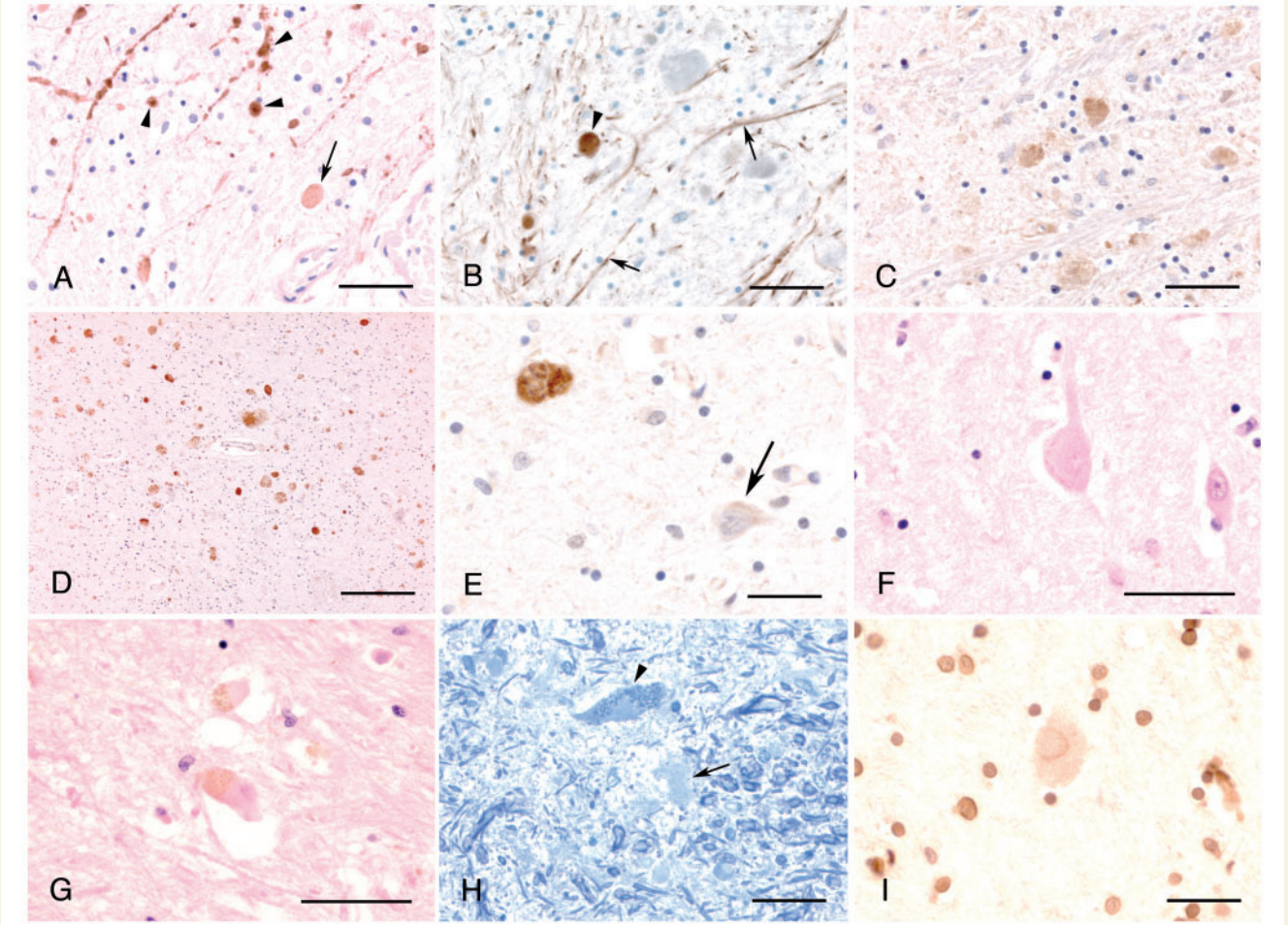

Figure 3 Features of neuroaxonal spheroids and degenerating neurons. (**A**) Immunohistochemistry for amyloid precursor protein demonstrates intense staining of neuroaxonal spheroids (arrowhead) and a lower amount of staining, or no staining, of degenerating neurons (arrow) in the globus pallidus in PKAN (scale: 50 μm). (**B**) Immunohistochemistry for high-molecular weight neurofilament protein reveals limited staining, mostly of smaller neuroaxonal spheroids (arrowheads), which are larger than residual axons (arrows), but significantly smaller than negatively staining degenerating neurons in the background (scale: 50 μm). (**C**) tau-2 immunohistochemistry reveals variable expression of tau in degenerating neurons; an area of relatively intense staining is depicted (scale: 50 μm). (**D**) The spectrum of degenerating neurons and neuroaxonal spheroids in the globus pallidus are uniformly positive by anti-ubiquitin immunohistochemistry (scale: 200 μm). (**E**) Higher magnification of ubiquitin immunohistochemistry of globus pallidus, showing strong granular staining of degenerating neurons (*upper left*) as well as finely granular cytoplasmic staining in rare intact neurons (arrow) (scale: 50 μm). (**F**) The neuron in the centre has developed eosinophilic cytoplasmic granularity and an indistinct nuclear contour compared with the intact neuron on the right (scale: 50 μm). (**G**) The lower neuron contains peripheral cytoplasmic lipofuscin pigment as well as paranuclear eosinophilic cytoplasm; the nucleus displays smudging. The upper neuron displays similar cytoplasmic changes but the nucleus has degenerated and is no longer apparent (magnification scale: 50 μm). (**H**) Toludine blue-stained plastic-embedded section of relatively intact (*upper*) and degenerated (*lower*) neurons in the globus pallidus. Neurons with advanced degeneration did not have morphologically recognizable nuclei or distinct cytoplasmic boundaries, however, small axons tended to be relatively preserved (scale: 50 μm). (**I**) Lamin A/C immunohistochemistry of structures showing advanced degeneration in the globus pallidus reveals a residual nuclear outline, indicating their cellular origin. Nuclear size indicates neuronal origin; note pallor of staining compared with surrounding viable glial nuclei (scale: 50 μm).

the age of subjects at death. Findings are summarized in Table 2, and the following comments pertain to specific findings in each case.

Case 20

Marked parenchymal rarefaction in the globus pallidus was noted in this case, but the degree of neuronal loss was less marked than in the other cases. Degenerating neurons, strongly positive for ubiquitin and weakly for tau, were seen in the globus pallidus, but these were also less abundant than in other cases. Neuroaxonal spheroids were detectable by amyloid precursor protein immunohistochemistry in the globus pallidus and in subcortical white matter. The associated gliosis was relatively mild. Iron deposition, centred in the globus pallidus, was more pronounced than in the index case and was similar to the degree observed in Case 23. The remainder of the microscopic examination was unremarkable.

Table 2 Comparison of histopathologic findings across cases of molecularly-confirmed PKAN

Case	Iron deposition	Spheroids	Ubiquitin positivity	tau-positivity	Neuronal degeneration
20	+ + +	+ +	+ + +	+	+
23	+ + +	+ + +	+ + +	+	+ + +
120	+ +	+	+ + +	+	+ +
146	+ +	+ +	+ + +	+	+ +
158	+ + +	+ +	+ + +	+	+ + +
367	+ +	+	+ + +	+	+ + +

Case 23

Abundant degenerating neurons, strikingly concentrated in the globus pallidus, were associated with parenchymal rarefaction, neuronal loss and gliosis. The marked iron deposition observed in this case was concentrated in the globus pallidus. Occasional degenerating neurons also appeared in the internal capsule adjacent to the globus pallidus pars externa, associated with mild deposition of iron. These degenerating neurons stained intensely for ubiquitin and weakly for tau. This case also featured a substantial number of neuroaxonal spheroids in the subcortical white matter associated with generalized myelin pallor in that region. The remainder of the cortex, deep grey nuclei, brainstem and cerebellum were unremarkable, without evidence of neuronal loss, Lewy bodies, spheroids or other inclusions.

Case 120

A limited amount of globus pallidus was available for examination. This showed a mild degree of iron deposition, and a localized area containing ubiquitin positive and less strongly tau positive degenerating neurons. Occasional neuroaxonal spheroids were seen. Other sections were unremarkable.

Case 158

Abundant degenerating neurons, staining intensely with ubiquitin and weakly for tau, were found almost exclusively in the globus pallidus. Less frequent neuroaxonal spheroids were noted. These spheroids were associated with rarefaction and loss of neuropil, neurons and mild gliosis. Moderate to marked deposition of iron was also centred in the globus palidus. The remainder of the brain was unremarkable.

Case 367

Abundant degenerating neurons associated with parenchymal rarefaction, neuronal loss and mild astrogliosis were most prominent in the medial putamen and also involved the globus pallidus. There was moderate iron deposition limited to the globus pallidus. Degenerating neurons stained intensely with ubiquitin and were weakly positive for tau. Occasional neuroaxonal spheroids were identified. The remainder of the brain showed no pathological abnormalities.

Discussion

Our findings indicate a remarkably selective neurodegenerative process in PKAN targeting the globus pallidus, consistent with MRI findings. In cases for which magnetic resonance images were available for review, there was an absolute correlation between the T_2 hypointensity noted on MRI and histological findings of iron deposition. Furthermore, the marked astrogliosis, microglial activation and overall parenchymal rarefaction observed within the medial globus pallidus would be expected to lead to high signal intensity on T_2-weighted MRI. The histological findings provide a basis for the 'eye of the tiger' pattern observed on MRI (Fig. 4).

Pantothenate kinase 2 localizes to the mitochondria (Hortnagel *et al*., 2003; Johnson *et al*., 2004), and catalyses a crucial step in the conversion of dietary pantothenate (Vitamin B5) into the cellular cofactor coenzyme A. The activity of pantothenate kinase 2 is negatively regulated by palmitoyl-CoA and acetyl-CoA (Kotzbauer *et al.,* 2005) and stimulated by palmitoylcarnitine (Leonardi *et al.,* 2007), suggesting a role in β-oxidation. Disruption of the *Drosophila* pantothenate kinase, dPANK in the 'fumble' model leads to a deleterious effect on the DNA damage response (Bosveld *et al.,* 2008), suggesting an important role for this conserved, tightly regulated system in maintaining cellular viability. The specific mechanism(s) by which defective pantothenate kinase 2 leads to neuronal degeneration, the formation of neuroaxonal spheroids, and iron deposition are still unclear.

Although pantothenate kinase 2 is ubiquitously expressed, and serves a central role in coenzyme A metabolism, PKAN primarily affects the CNS. There are occasional peripheral manifestations of disease (e.g. testicular pathology, lipid profile abnormalities, acanthocytosis) without systemic iron deposition, which was again confirmed in the present study. We found that pathology is limited largely to the globus pallidus, although adjacent structures (medial putamen, internal capsule) and subcortical white matter are affected to a lesser degree. This specificity is remarkable given the ubiquitous expression of pantothenate kinase 2 and the central metabolic role of coenzyme A. In the present study, we have characterized important histological features of this unusual and highly selective degeneration, providing a framework for future studies that may begin to shed light on these phenomena.

Previous reports have described both large and small 'spheroid bodies' in NBIA (Malandrini *et al.,* 1996). In this study, we have clarified that the larger abnormal structures represent degenerating

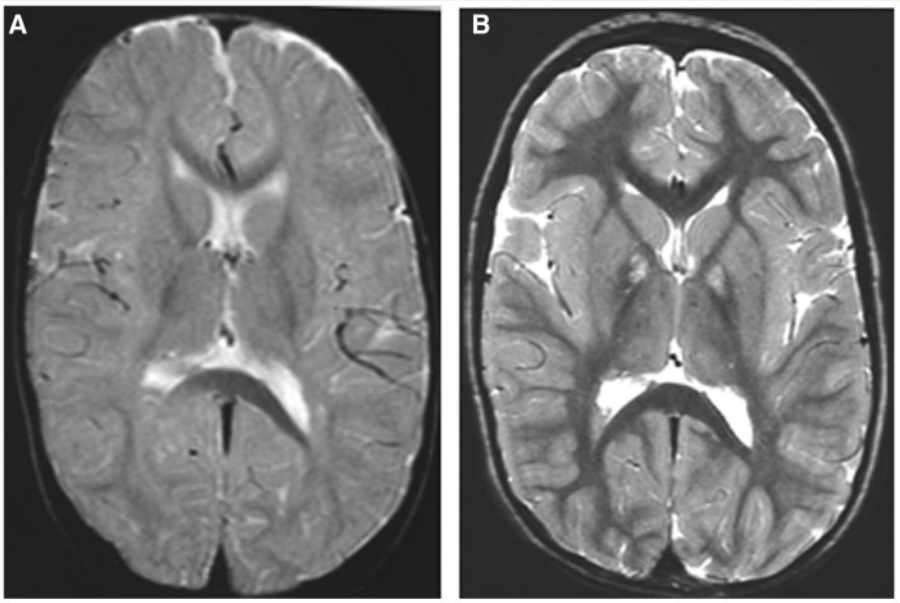

Figure 4 MRI evolution in PKAN. (**A**) Axial T_2-weighted sequence image taken from Case 120 taken when only mild gait impairment was present. (**B**) T_2-weighted image from Case 120 when the patient was fully symptomatic. The globus pallidus demonstrates the characteristic region of central signal hyperintensity with surrounding signal hypointensity known as the 'eye of the tiger.'

neurons, and we refer to them as such. In addition, neuroaxonal spheroids, which represent a non-specific form of axonal degeneration, were present in all of our cases. Although some expression of tau was observed within some degenerating neurons, the relatively faint immunoreactivity compared with that encountered in neurofibrillary tangles of Alzheimer's disease or other tauopathies such as progressive supranuclear palsy indicated that tau is not a consistent or major component of these inclusions and that other, as yet unidentified protein(s) contribute to them. Conversely, the intensity of ubiquitin staining indicates prominent accumulation of an abnormal protein, but the identity of this protein remains to be elucidated. Despite the degree of neurodegeneration that is present, there is remarkably little inflammatory response aside from infiltrates of iron-containing macrophages and limited astrogliosis and microglial activation.

The distribution of histopathological lesions in our cases is more limited than that seen in the NBIA subtype phospholipase-associated neurodegeneration (Paisan-Ruiz *et al.,* 2010). In phospholipase-associated neurodegeneration, spheroids, gliosis and neuronal loss are found in the globus pallidus as well as in the substantia nigra pars reticularis, cerebellar white matter, nucleus gracilis and dentate nucleus. Previous reports have suggested that PKAN could be characterized as both a synucleinopathy and tauopathy (Galvin *et al.,* 2000; Neumann, *et al.,* 2000; Wakabayashi *et al.,* 2000). However, our studies, performed in patients with molecularly confirmed PKAN, demonstrate a fundamentally different histological phenotype. Notably, Lewy bodies and other abnormalities in α-synuclein were not seen in any of our cases. Neurofibrillary tangles and tau-positive neurites were also absent from our series.

The lack of α-synuclein pathology distinguishes PKAN from phospholipase-associated neurodegeneration (Paisan-Ruiz *et al.,* 2010) and challenges earlier reports. This finding suggests that despite common features of globus pallidus iron deposition, neuroaxonal spheroids, prominent dystonia and intellectual decline, PKAN and phospholipase-associated neurodegeneration exhibit fundamental differences at the histological and, by extension, molecular level. Prior studies have also suggested ultrastructural differences in spheroid composition between PKAN and phospholipase-associated neurodegeneration (Malandrini *et al.,* 1995). Bras *et al.* (2008) proposed that both PKAN and phospholipase-associated neurodegeneration are primary synucleinopathies, united by a common abnormality of ceramide metabolism. The recognition that synuclein pathology is not a feature of PKAN requires modification of this model, although ceramide metabolism may still be relevant for NBIA and PKAN (Kruer *et al.,* 2010).

The aetiology of iron deposition in PKAN remains unknown and a potential link to aberrant lipid metabolism remains cryptic. In the present studies, we identified iron deposition in the cytoplasm of neurons, glia, macrophages (especially in a perivascular distribution), and increased diffusely in the neuropil of the globus pallidus ('iron dust'). There was imperfect agreement between iron identified by Perls' stain and the pattern of ferritin staining, clearly indicating that iron exists in other forms as well. Iron-laden macrophages were prominent in all cases examined, suggesting an attempt to remove iron from the brain parenchyma. The identification of increased amyloid precursor protein staining, both in neuroaxonal spheroids and in neuronal processes, is intriguing, especially given the recent recognition of ferroxidase activity in amyloid precursor protein (Duce *et al.,* 2010). Such a role in cellular iron efflux may be relevant in states of iron overload or maldistribution. The pathophysiological mechanisms underlying

iron deposition continue to be of great interest, particularly given the finding of iron accumulation in other neurodegenerative disorders, including Alzheimer's (Schenck *et al.,* 2006) and Parkinson's (Wallis *et al.,* 2008) diseases and multiple system atrophy (von Lewinsky *et al.,* 2007). For these reasons, the characterization of the mechanisms underlying iron deposition represents an important priority for the field and one that remains a focus of ongoing investigation (Poli *et al*., 2010).

Acknowledgements

The authors thank the patients and families whose selfless donation made this work possible. The authors thank the NICHD, Brain and Tissue Bank for Developmental Disorders at the University of Maryland, Baltimore, MD for providing access to the tissue used in this study. The role of NICHD, Brain and Tissue Bank is to distribute tissue, and, therefore, cannot endorse the studies performed or the interpretation of results. The authors also thank S. Westaway, S. Richards and M. Johnson for help in performing *PANK2* sequence analysis and E. Haverfield and S. Das for their assistance in performing MLPA analyses.

Funding

NBIA Disorders Association (to S.J.H. and M.C.K.) and Associazione Italiana Sindromi Neurodegenerative da Accumulo di Ferro (to M.C.K.); American Academy of Neurology (Clinical Research Training Fellowship to M.C.K.); American Philosophical Society (Daland Award to M.C.K.); Medical Research Foundation of Oregon (to M.C.K.); and the National Institutes of Health [Pediatric Loan Repayment Program award UWXY3099 (to M.C.K.)] and P30AG008017 (to D.C. and R.L.W.); Oregon Clinical and Translational Research Institute (OCTRI; NCRR grant UL1 RR024140).

References

Bras J, Singleton A, Cookson MR, Hardy J. Emerging pathways in genetic Parkinson's disease: Potential role of ceramide metabolism in Lewy body disease. FEBS J 2008; 275: 5767–73.

Bosveld F, Rana A, van der Wouden PE, Lemstra W, Ritsema M, Kampinga HH, et al. De novo CoA biosynthesis is required to maintain DNA integrity during development of the Drosophila nervous system. Hum Mol Genet 2008; 17: 2058–69.

Dooling EC, Schoene WC, Richardson EP Jr. Hallervorden-Spatz syndrome. Arch Neurol 1974; 30: 70–83.

Duce JA, Tsatsanis A, Cater MA, James SA, Robb E, Wikhe K, et al. Iron-export ferroxidase activity of β-amyloid precursor protein is inhibited by zinc in Alzheimer's disease. Cell 2010; 142: 857–67.

Egan RA, Weleber RG, Hogarth P, Gregory A, Coryell J, Westaway SK, et al. Neuro-ophthalmologic and electroretinographic findings in pantothenate kinase-associated neurodegeneration (formerly Hallervorden-Spatz syndrome). Am J Ophthalmol 2005; 140: 267–74.

Freeman K, Gregory A, Turner A, Blasco P, Hogarth P, Hayflick S. Intellectual and adaptive behaviour functioning in pantothenate kinase-associated neurodegeneration. J Intellect Disabil Res 2007; 51 (Pt. 6): 417–26.

Galvin JE, Giasson B, Hurtig HI, Lee VM, Trojanowski JQ. Neurodegeneration with brain iron accumulation, type 1 is characterized by alpha-, beta-, and gamma-synuclein neuropathology. Am J Pathol 2000; 157: 361–8.

Gregory A, Polster BJ, Hayflick SJ. Clinical and genetic delineation of neurodegeneration with brain iron accumulation. J Med Genet 2009; 46: 73–80.

Halliday W. The nosology of Hallervorden-spatz disease. J Neurol Sci 1995; 134 (Suppl): 84–91.

Hardy J, Lewis P, Revesz T, Lees A, Paisan-Ruiz C. The genetics of Parkinson's syndromes: a critical review. Curr Opin Genet Dev 2009; 19: 254–65.

Haverfield EV, Whited AJ, Petras KS, Dobyns WB, Das S. Intragenic deletions and duplications of the LIS1 and DCX genes: a major disease-causing mechanism in lissencephaly and subcortical band heterotopia. Eur J Hum Genet 2009; 17: 911–8.

Hayflick SJ, Westaway SK, Levinson B, Zhou B, Johnson MA, Ching KHL, et al. Genetic, clinical and radiographic delineation of Hallervorden-Spatz syndrome. NEJM 2003; 1348: 33–40.

Hörtnagel K, Prokisch H, Meitinger T. An isoform of hPANK2, deficient in pantothenate kinase-associated neurodegeneration, localizes to mitochondria. Hum Mol Genet 2003; 12: 321–7.

Johnson MA, Kuo YM, Westaway SK, Parker SM, Ching KH, Gitschier J, et al. Mitochondrial localization of human PANK2 and hypotheses of secondary iron accumulation in pantothenate kinase-associated neurodegeneration. Ann NY Acad Sci 2004; 1012: 282–98.

Kitis O, Tekgul H, Erdemir G, Polat M, Serdaroglu G, Tosun A, et al. Identification of axonal involvement in Hallervorden-Spatz disease with magnetic resonance spectroscopy. J Neuroradiol 2006; 33: 129–32.

Kotzbauer PT, Truax AC, Trojanowski JQ, Lee VM. Altered neuronal mitochondrial coenzyme A synthesis in neurodegeneration with brain iron accumulation caused by abnormal processing, stability, and catalytic activity of mutant pantothenate kinase 2. J Neurosci 2005; 25: 689–98.

Kruer MC, Paisán-Ruiz C, Boddaert N, Yoon MY, Hama H, Gregory A, et al. Defective FA2H leads to a novel form of neurodegeneration with brain iron accumulation (NBIA). Ann Neurol 2010; 68: 611–8.

Leonardi R, Rock CO, Jackowski S, Zhang YM. Activation of human mitochondrial pantothenate kinase 2 by palmitoylcarnitine. Proc Natl Acad Sci USA 2007; 104: 1494–9.

Malandrini A, Cavallaro T, Fabrizi GM, Berti G, Salvestroni R, Salvadori C, et al. Ultrastructure and immunoreactivity of dystrophic axons indicate a different pathogenesis of Hallervorden-Spatz disease and infantile neuroaxonal dystrophy. Virchows Arch 1995; 427: 415–21.

Malandrini A, Fabrizi GM, Bartalucci P, Salvadori C, Berti G, Sabò C, et al. Clinicopathological study of familial late infantile Hallervorden-Spatz disease: a particular form of neuroacanthocytosis. Childs Nerv Syst 1996; 12: 155–60.

Meguro R, Asano Y, Odagiri S, Li C, Iwatsuki H, Shoumura K. Nonheme-iron histochemistry for light and electron microscopy: a historical, theoretical and technical review. Arch Histol Cytol 2007; 70: 1–19.

Neumann M, Adler S, Schlüter O, Kremmer E, Benecke R, Kretzschmar HA. Alpha-synuclein accumulation in a case of neurodegeneration with brain iron accumulation type 1 (NBIA-1, formerly Hallervorden-Spatz syndrome) with widespread cortical and brainstem-type Lewy bodies. Acta Neuropathol 2000; 100: 568–74.

Paisán-Ruiz C, Li A, Schneider SA, Holton JL, Johnson R, Kidd D, et al. Widespread Lewy body and tau accumulation in childhood and adult onset dystonia-parkinsonism cases with PLA2G6 mutations. Neurobiol Aging 2010 [Epub ahead of print].

Poli M, Derosas M, Luscieti S, Cavadini P, Campanella A, Verardi R, et al. Pantothenate kinase-2 (Pank2) silencing causes cell growth reduction, cell-specific ferroportin upregulation and iron deregulation. Neurobiol Dis 2010; 39: 204–10.

Saito Y, Kawai M, Inoue K, Sasaki R, Arai H, Nanba E, et al. Widespread expression of alpha-synuclein and tau immunoreactivity in

Hallervorden-Spatz syndrome with protracted clinical course. J Neurol Sci 2000; 177: 48–59.

Schenck JF, Zimmerman EA, Li Z, Adak S, Saha A, Tandon R, et al. High-field magnetic resonance imaging of brain iron in Alzheimer disease. Top Magn Reson Imaging 2006; 17: 41–50.

Shevell MI, Peiffer J. Julius Hallervorden's wartime activities: implications for science under dictatorship. Pediatr Neurol 2001; 25: 162–5.

von Lewinski F, Werner C, Jörn T, Mohr A, Sixel-Döring F, Trenkwalder C. T2*-weighted MRI in diagnosis of multiple system atrophy. A practical approach for clinicians. J Neurol 2007; 254: 1184–8.

Wakabayashi K, Fukushima T, Koide R, Horikawa Y, Hasegawa M, Watanabe Y, et al. Juvenile-onset generalized neuroaxonal dystrophy (Hallervorden-Spatz disease) with diffuse neurofibrillary and lewy body pathology. Acta Neuropathol 2000; 99: 331–6.

Wallis LI, Paley MN, Graham JM, Grünewald RA, Wignall EL, Joy HM, et al. MRI assessment of basal ganglia iron deposition in Parkinson's disease. J Magn Reson Imaging 2008; 28: 1061–7.

Zarranz JJ, Gómez-Esteban JC, Atarés B, Lezcano E, Forcadas M. Tau-predominant-associated pathology in a sporadic late-onset Hallervorden-Spatz syndrome. Mov Disord 2006; 21: 107–11.

Zhou B, Westaway SK, Levinson B, Johnson MA, Gitschier J, Hayflick SJ. A novel pantothenate kinase gene (PANK2) is defective in Hallervorden-Spatz syndrome. Nat Genet 2001; 28: 345–9.